ACS Catalysis

Research Article

pubs.acs.org/acscatalysis

Detecting the Genesis of a High-Performance Carbon-Supported Pd Sulfide Nanophase and Its Evolution in the Hydrogenation of Butadiene

Belén Bachiller-Baeza,[†] Ana Iglesias-Juez,[†] Eva Castillejos-López,[‡] Antonio Guerrero-Ruiz,*[,‡] Marco Di Michiel,[§] Marcos Fernández-García,[†] and Inmaculada Rodríguez-Ramos*[,†]

[†]Instituto de Catálisis y Petroleoquímica, CSIC, C/Marie Curie 2, 28049 Madrid, Spain

[‡]Departamento de Química Inorgánica y Química Técnica, UNED, C/Senda del Rey 9, 28040 Madrid, Spain

[§]ESRF, 6 Rue Jules Horowitz, 38043 Grenoble, France

Supporting Information

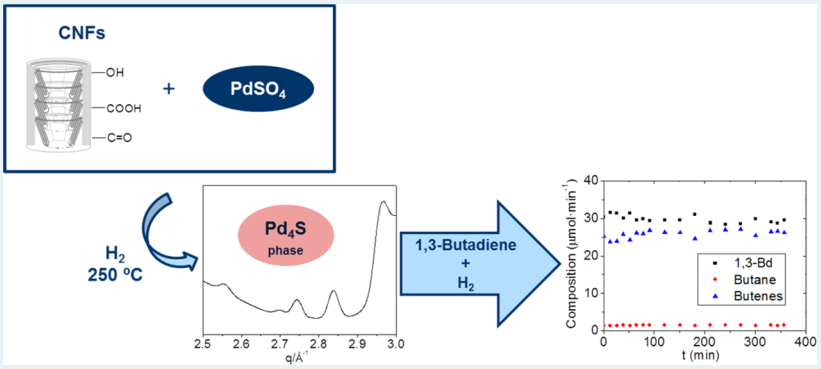

ABSTRACT: A new procedure for preparation of palladium sulfide nanoparticles, which are deposited and anchored over highly graphitized carbon nanofibers, is presented. The preparation method is based on the use of $PdSO_4$ as metal precursor or alternatively in the previous functionalization of the carbon surfaces with sulfonic groups by treatment with fuming sulfuric acid. Using an in situ high-energy X-ray diffraction technique, in both cases it is demonstrated that during the reduction treatment, the initially present palladium hydride is transformed into a palladium sulfide (Pd_4S). The catalytic properties of these materials have been tested in the gas-phase butadiene partial reduction to butenes. Although metallic palladium nanoparticles supported in the same carbon fibers produce butane as the principal product, the supported Pd_4S nanocrystals mainly yield different isomers of butenes independently of the conversion level. Furthermore, applying the same X-ray diffraction method reveals that this catalytic phase is stable during reaction.

KEYWORDS: *catalyst synthesis, palladium sulfide, X-ray diffraction, hydrogenation reaction, structure−activity relationship*

1. INTRODUCTION

Partial hydrogenation of alkynes and alkadienes in the presence of alkenes is one of the most important processes in the chemical industry, and selectivity is a relevant issue.[1] Supported palladium catalysts are currently used for the hydrogenation of 1,3-butadiene, but because they lack selectivity to the desired n-butenes when the ratio of monoalkenes to dienes is high, promoters (Ag, Au, Ga, or Cu) or modifiers (CO or sulfur) are needed to enhance the yield of partially hydrogenated products.[2−6] The reaction is known to be structure-sensitive,[7,8] and it has been reported that Pd catalysts under reaction can accommodate carbon atoms in subsurface layers that affect the hydrogen diffusion, thereby improving the alkene selectivity.[9]

The use of carbon materials as supports of metal nanoparticles is widely employed for preparing heterogeneous catalysts, among others, because as a consequence of the moderate metal−graphite interaction, new chemical compositions can be easily synthesized, that is, intermetallic compounds[S] or transition metal sulfides.[10] In addition, modification of the carbon surface with functionalities has been used for anchoring metal nanoparticles to the carbon surface.[11,12]

Supported palladium sulfides catalysts are generally synthesized through presulfidation of supported Pd metal catalysts using H_2S, Na_2S, or organic sulfur-containing molecules,[10,13] but such methods have the problems of high environmental pollution and scaling cost.[1,3] Recently, thiolate self-assembled monolayers were used to block specific active sites on Pd/Al_2O_3 during the hydrogenation of furfural.[14] The adsorbed thiolate modifiers serve the role of isolating certain highly active sites

Received: April 30, 2015
Revised: July 22, 2015
Published: July 28, 2015

DOI: 10.1021/acscatal.5b00896
ACS Catal. 2015, 5, 5235−5241

for hydrodeoxygenation reaction, restricting selectivity toward undesired products. Moreover, preformed palladium sulfide nanoparticles grafted on graphene oxide (GO) have been reported for catalysis of the Suzuki coupling reaction.[15] In this latter case, the Pd sulfide nanoparticles were prepared by thermolysis of an organometallic precursor containing Pd−S bonds. This method reduces the toxicity risks and contamination. However, the palladium sulfide/GO composite suffers significant leaching of the active Pd during the catalytic reaction, which hinders its recyclability. Therefore, it seems necessary to develop new, simple, and safe methods to synthesize supported palladium catalysts and obtain more detailed insight into their evolution and stability under reaction conditions.

Herein, we present a study showing the formation and the evolution under reaction conditions of Pd sulfide nanoparticles supported on carbon nanofibers by coupling time-resolved high-energy X-ray diffraction (HEXRD) and mass spectrometry (MS). This approach allows us to simultaneously investigate, in a time-resolved manner, the structure−activity relationship of the supported Pd nanoparticles, as well as the compounds that are formed or converted over them.[16] We characterize the nature of the Pd-based nanoparticles generated by reduction under hydrogen flow at 250 °C of two metal precursors, Pd chloride and Pd sulfate, deposited (1 wt % of Pd) on carbon nanofibers functionalized with sulfonic or carboxylic groups, respectively. Also, we study the evolution of these Pd-based catalysts under butadiene hydrogenation reaction conditions.

2. EXPERIMENTAL SECTION

Preparation of Carbon Supports. A commercial carbon nanofiber was used in this study: Pyrograph III PR24-HHT (SBET = 32 m^2/g) provided by Applied Sciences Inc. The PR24-HHT fibers (denoted as HHT) were originally treated at high temperature (∼3030 °C), possess a stacked-cup morphology with a hollow core through the length of the fiber, and also present a jagged outer surface with "round heads" or "loop" structures, which connect several layers.[17]

HHT was functionalized according to reported procedures yielding HHTox.[18] Briefly, parent carbon nanofiber was refluxed in 50% nitric acid (carbon/HNO_3 = 1 g/10 mL) at 100 °C for 48 h in order to increase the concentration of functional groups on the surface. HHT was also subjected to a sulfonation treatment.[19] Aliquots of 3 g of fibers were immersed in 150 mL of fuming sulfuric acid (15 wt % SO_3) at 80 °C under a nitrogen gas atmosphere for 7 h. After the treatment, the suspension was washed with deionized water to remove any excess sulfuric acid in the carbon nanomaterial, filtered, and dried at 120 °C. The resulting modified sample was labeled HHT-SO_3H. Elemental chemical analysis of carbon, hydrogen, and sulfur was carried out in a LECO CHNS-932 instrument. The results reveal a 1 wt % content of sulfur.

Catalyst Preparation. Catalysts were prepared by incipient wetness impregnation of the supports with water solutions of $PdCl_2$ or $PdSO_4$. The catalysts were prepared with a 1 wt % Pd loading. In the case of $PdCl_2$, the precursor was dissolved in concentrated HCl to generate tetrachloride palladium acid (H_2PdCl_4), heated to eliminate chlorine, dissolved in distilled water, dried, and again diluted in water until the final volume was reached. This solution was dropped to the carbon nanofiber supports (HHTox and HHT-SO_3H).

Characterization Details. The chemical nature of the functional groups of the two supports was evaluated by temperature-programmed desorption coupled with mass spectrometer (TPD-MS) experiments under vacuum in a conventional volumetric apparatus connected to a RGA-200 SRS mass spectrometer.[20] The sample was evacuated for 30 min at room temperature and then ramped to 1023 K at a 10 K min^{-1} rate.

All the samples were characterized by X-ray photoelectron spectroscopy (XPS), thermogravimetry, and transmission electron microscopy (TEM) analyses. X-ray photoelectron spectra of the supports and catalysts were recorded with an ESCA-PROBE P (Omicron) spectrometer by using non-monochromatized Mg Kα radiation (1253.6 eV). The binding energy of Pd 3d and S 2p were internal referenced to the C 1s line at 284.6 eV. The error in determination of electron binding energies did not exceed 0.2 eV. Each sample was pressed into a small pellet of 15 mm diameter and placed in the sample holder and degassed in the chamber for 6−8 h to achieve a dynamic vacuum below 10−8 Pa before analysis. The spectral data for each sample was analyzed using CASA XPS software. The relative concentrations and atomic ratios were determined from the integrated intensities of photoelectron lines corrected for the corresponding atomic sensitivity factor.

Transmission electron microscopy (TEM) images of the catalysts were measured using a JEOL JEM-2100 field-emission gun electron microscope operated at 200 kV. The samples were ground, ultrasonically suspended in ethanol, and then dripped onto a carbon-coated copper grid before TEM images were generated. The mean diameter (d) of the Pd particle size were calculated on the basis of a minimum of 100 particles.

High-energy X-ray diffraction (HEXRD) data were collected at the ID15A beamline at the ESRF-The European Synchrotron with a wavelength of 0.17750 Å (69.85 keV), using a PerkinElmer area detector and a sample−detector distance of 650 mm. The diffraction patterns were collected with an exposure time of 30 s. Diffraction data were fitted using the Rietveld method with the XPert Highscore Plus program (Panalytical). The reactor and heat gun were mounted on a Huber stage capable of translations in the *x*, *y*, and *z* directions. The carbon fibers supported catalysts were pressed into pellets and sieved to a size of 0.075 to 0.150 mm. Aliquots of these pellet samples were loaded in a fixed bed quartz tube of 2 mm internal diameter, located between two glass wools. The flow of reaction gases feed to the reactor was constant at 20 mL·min^{-1}, with compositions of 15% hydrogen in helium during temperature-programmed reduction experiments and 15% hydrogen + 3% butadiene in helium during hydrogenation reaction conditions. H_2/H_2 + Bd/H_2 alternate exposures at constant increasing temperatures were applied with an exposure time of 30 min for each atmosphere. The reactor was heated with one Leister LE mini heat gun fitted with a heat spreader. The temperature inside the catalytic bed was measured using a thermocouple inserted into the carbon-supported sample. The range of operation temperatures was from room temperature up to 550 K. The exhaust products from the reactor were analyzed using a European Spectrometry ecoSyst-P Man-Portable mass spectrometer with capillary inlet and heated inlet tubes.

Catalytic Measurements. Steady-state catalytic experiments for butadiene (Bd) hydrogenation were carried out in a continuous-flow fixed-bed reactor (4 mm inner diameter). Before reaction, the catalyst was pretreated in flowing H_2 at 250

DOI: 10.1021/acscatal.5b00896
ACS Catal. 2015, 5, 5235−5241

°C for 1 h. The reactants H_2 (10% vol) and Bd (2% vol) with the balance of N_2 passed through the catalyst bed at a total flow rate of 60 mL/min. The hydrogen amount was in large excess. Any significant mass-transfer limitation was precluded by using this high linear velocity and powder (sieve fraction 150−250 μm) catalysts. The occurrence of external diffusion limitations was ruled out by running tests where both the flow rate and the catalyst amount were significantly changed while keeping the mass/flow rate ratio constant (8.3×10^{-6} g·h/ml). The reaction temperature was varied between room temperature and 473 K at atmospheric pressure. The reactor effluent was online analyzed using a gas Varian 3400 gas chromatograph with flame ion detector (FID) and thermal conductivity detector (TDC) with a 20% BMEA Chromosorb P80/100 column.

3. RESULTS AND DISCUSSION

Table 1 summarizes the performance of the $PdCl_2$−HHT-SO_3H and $PdSO_4$−HHTox catalysts in the selective hydrogenation of butadiene (Bd) obtained in a fixed bed reactor with the reaction mixture of H_2:Bd:N_2 of 10:2:88. The $PdCl_2$−HHTox sample is included as a reference for comparison. This latter catalyst displays high activity (100% conversion of butadiene is reached at room temperature) but is totally unselective to partial hydrogenation, as butane was the only product. However, when sulfur is initially present in the catalyst precursor, either as surface sulfonic groups on the support or as moieties coming from the Pd precursor, the reduced catalyst (250 °C-2h in hydrogen) shows high selectivity for the hydrogenation of butadiene to butenes (99% of butenes in the case of $PdSO_4$−HHTox at 100% conversion), although the activity is somewhat reduced as the selectivity increases from $PdCl_2$−HHT-SO_3H to $PdSO_4$−HHTox. Clearly, the presence of the sulfur modifier has to be related with the selective performance of the $PdCl_2$−HHT-SO_3H and $PdSO_4$−HHTox catalysts, especially in the last case. Such marked changes in selectivity require further investigation.

Table 1. Results Characterizing the Performance of Pd Catalysts in the Selective Hydrogenation of Butadiene[a]

sample	T_{30} (°C)	T_{100} (°C)	S_{30} (%)	S_{100} (%)
$PdCl_2$−HHTox	-	25	0	0
$PdSO_4$−HHTox	120	150	99	99
$PdCl_2$−HHT-SO_3H	100	120	99	75

[a] T_{30} and T_{100}, temperature at which the 30% and 100% conversion of butadiene is achieved. S_{30} and S_{100}, selectivity toward partial hydrogenation at 30% and 100% conversion. Reaction performed in a fixed bed reactor with the reaction mixture of H_2:Bd:N_2 of 10:2:88, 30 mg catalyst.

Figure 1 presents the HRTEM pictures and histograms with the size distribution of palladium particle diameters for the different catalysts reduced at 250 °C. A broad range of particle sizes and a relative regular distribution of the Pd particles over the support are observed for the distinct catalysts. Both features can arise from the high graphitization degree and low defect density produced by surface functionalization of the support. However, the particle size distribution is shifted toward smaller sizes for the catalysts containing sulfur in the catalyst precursor. Thus, between 65 and 75% of the metallic particles in $PdSO_4$−HHTox and $PdCl_2$−HHT-SO_3H catalysts have diameters below 4 nm. The micrographs (Figure 1 and Figures S2−S4 in Supporting Information) show the spherical nature of the Pd particles for the different catalysts, particularly for the $PdCl_2$−HHTox, which, as mentioned, could be consequence of a weak interaction between the particles and the nanofibers.

The mean particle diameters (d) of Pd calculated from TEM measurements of the different samples are displayed in Table 2. The mean volume particle diameters ($d_{4/3}$) were also estimated and included in Table 2. The mean volume particle diameter, sensitive to the volume of particles, gives more weight to the larger particles and is more appropriate than mean particle size

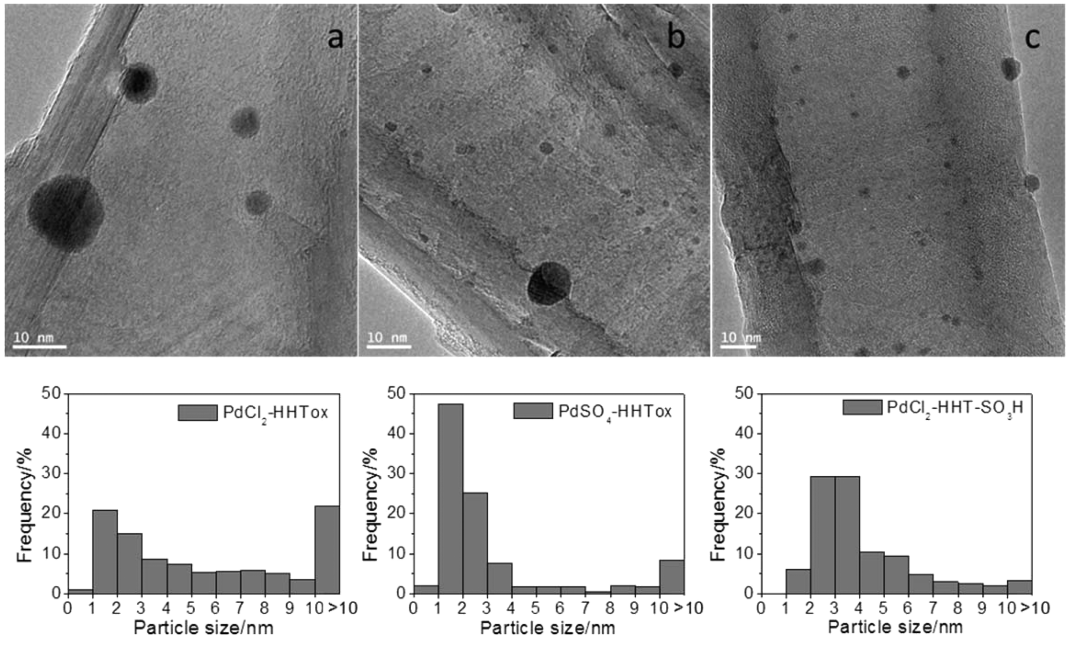

Figure 1. HRTEM micrographs and histograms with the size distribution of particle diameters for (a) $PdCl_2$−HHTox, (b) $PdSO_4$−HHTox, and (c) $PdCl_2$−HHT-SO_3H catalysts reduced at 250 °C.

DOI: 10.1021/acscatal.5b00896
ACS Catal. 2015, 5, 5235−5241

Table 2. Mean Particle Size (d) and Volume-Surface Mean Particle Size ($d_{4/3}$) Estimated from TEM Measurements

catalyst	$\Sigma n_i d_i / \Sigma n_i$ (nm)	$\Sigma n_i d_i^4 / \Sigma n_i d_i^3$ (nm)
$PdCl_2$−HHTox	6.6	18.3
$PdSO_4$−HHTox	4.6	17.1
$PdCl_2$−HHT-SO_3H	4.2	8.5

for comparison with data obtained from physical techniques such as X-ray line broadening or magnetic methods.

Characterization under realistic reaction conditions of supported nanoparticles with a range of sizes of Pd nanoparticles and mean size around 4.5 nm (from TEM measurements) is not an easy task because few methods can be applied to this type of materials. Conventional X-ray diffraction techniques (XRD) performed in a laboratory diffractometer do not provide useful information on low-loading metal-supported catalysts because of the low signal intensity. In contrast, using synchrotron-based radiation, the high energy X-ray diffraction (HEXRD) can provide structural information on finely dispersed palladium on catalysts under reaction conditions. Physical methods, such as high-resolution transmission electron microscopy (HRTEM), fail when these nanoparticles have to be studied in situ in a catalyzed reaction. In fact, HRTEM measurements should be performed under high vacuum conditions. In addition, it is important to consider that statistical measurements of microdiffraction over a large number of particles are difficult to achieve.

To investigate the nature of the Pd-based nanoparticles in the different catalysts during the temperature-programmed reduction in hydrogen, we use HEXRD coupled with MS. Color map representation in Figure 2 shows the variation of the HEXRD patterns for the Pd catalysts from room temperature to 250 °C.

When the $PdCl_2$−HHTox sample (upper panel) is exposed to hydrogen/helium at room temperature, the HERXD pattern reveals the formation of the β phase of Pd hydride (peak (111) at 2.70 $Å^{-1}$).[21] Heating to higher temperature, it is seen that above 90 °C, the most intense (111) reflection shifts to a higher Q value (2.80 $Å^{-1}$) due to the lattice contraction as hydrogen is released from the hydride phase to form metallic Pd (lattice constant at 250 °C, a = 3.904 Å).

The structural evolution of the sample prepared with palladium sulfate ($PdSO_4$−HHTox, middle panel) is different after the transformation into metallic Pd at 90 °C, because as the temperature approaches 150 °C, a second transformation occurs, resulting in the formation of the Pd_4S phase ((210) and (112) peaks at 2.74 and 2.83 $Å^{-1}$, respectively).[22] The formation of the Pd sulfide phase is further described with the help of MS. In Figure 2, as an inset onto color maps, selected MS signals labeled m/z = 34 and m/z = 64 are plotted. The first one is associated with H_2S, whereas the m/z = 64 corresponds to SO_2. Both products stem as main gas residues coming from the decomposition/reduction of the sulfate anions of the metal precursor deposited on the support and appear with a constant level from 100 to 160 °C. At this latter temperature, Pd is completely transformed to the single well-crystallized Pd_4S structure (lattice constants at 250 °C, a = 5.137 Å, c = 5.623 Å). Although sulfidation of supported metallic palladium with H_2S or Na_2S usually leads to mixed crystal phases, formation of a single phase seems to be favored when Pd is supported on carbon.[10] The formation of palladium sulfides supported on carbon is highly dependent on the

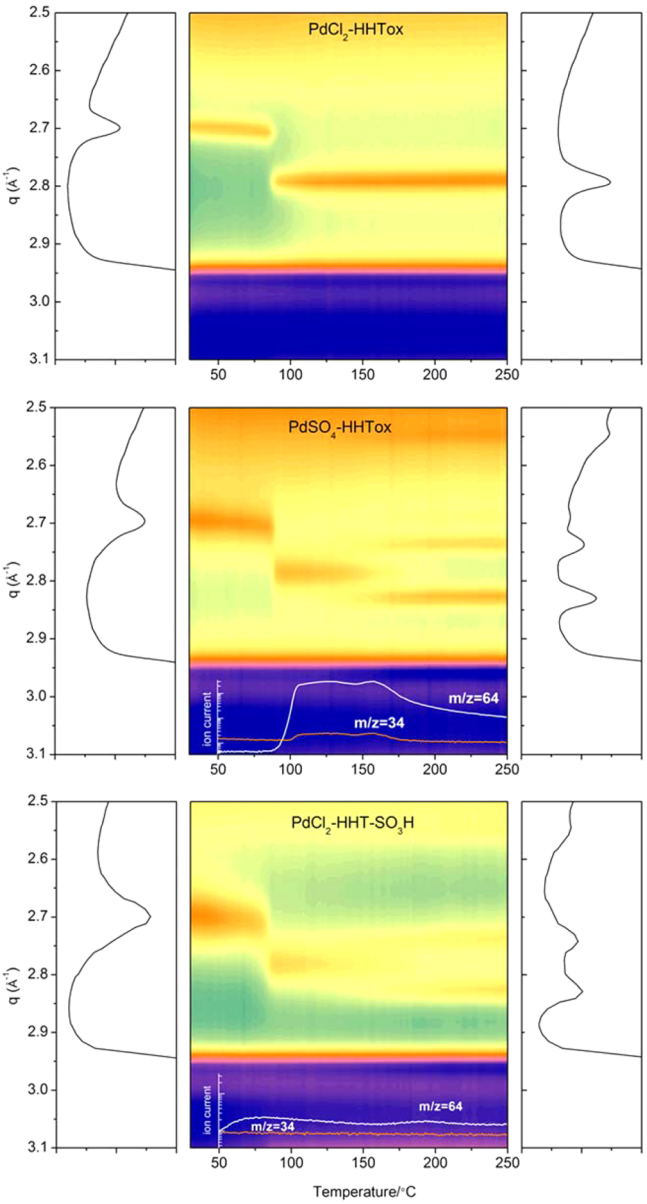

Figure 2. Intensity contour maps of the HEXRD patterns obtained during temperature-programmed reduction in hydrogen/helium from room temperature up to 250 °C. Initial and final HEXRD patterns are shown on the left and right of panels, respectively. MS (m/z = 34 and 64) analysis of gases evolved during the heating treatment is shown in the blue graph insets.

composition of the sufidation atmosphere and temperature. Single-phase Pd_4S was reported at 150 °C under H_2S/H_2 ratios between 0.008 and 0.25.[10,23]

In the case of the $PdCl_2$−HHT-SO_3H (lower panel), the complete transformation of β phase of Pd hydride to Pd is observed at 90 °C. From 150 °C and up to 250 °C, only part of the Pd metal is transformed to Pd_4S (lattice constants, a = 5.136 Å, c = 5.619 Å). The presence of a minor metallic Pd phase is successfully tracked out in the high-resolution XRD patterns presented in Figure 2 (bottom). HEXRD fitting using the Rietveld method reveals that a 21 wt % of metallic Pd remains (see Supporting Information, Table S1). From the MS analysis (inset, lower panel), we learn that the evolution of H_2S and SO_2 is appreciably lower than for the $PdSO_4$−HHTox sample and clearly not enough to transform the whole metallic

DOI: 10.1021/acscatal.5b00896
ACS Catal. 2015, 5, 5235−5241

Pd into Pd_4S. Both fresh samples, $PdSO_4$−HHTox and $PdCl_2$−HHT-SO_3H, have similar initial sulfur content, 1 wt % SO_4 and 1 wt % SO_3H, respectively.

Surface chemical analysis by XPS of fresh samples clearly evidenced the presence of sulfur on the surface, because the characteristic peak stemming from the overlapped S $2p_{3/2}$ and S $2p_{1/2}$ doublet (spin−orbit splitting of 1.2. eV, see Figure S7 in Supporting Information) was revealed at around 169 eV, which is characteristic of sulfate (Figure 3) and −SO_3H groups (result

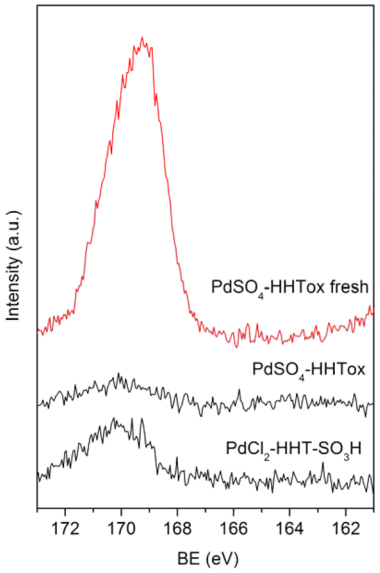

Figure 3. XPS spectra of the S 2p core level for the $PdSO_4$−HHTox and $PdCl_2$−HHT-SO_3H catalysts reduced at 250 °C and the fresh $PdSO_4$−HHTox.

not shown). After reduction at 250 °C, the XPS spectra show that the $PdCl_2$−HHT-SO_3H sample still has sulfonic groups on the surface while the surface of $PdSO_4$−HHTox sample is practically free of sulfur. Moreover, no S 2p peaks emerging from sulfide or S_n species, expected at 161.5 and 163.5−164 eV respectively, were found.[13]

The XPS spectra for the doublet Pd 3d5/2 and 3d3/2 of the fresh $PdSO_4$−HHTox and the $PdSO_4$−HHTox and $PdCl_2$−HHT- SO_3H catalysts reduced at 250 °C are shown in Figure 4. It is observed that the Pd 3d5/2 peak shifts from 337.3 eV (Pd^{2+} in the $PdSO_4$−HHTox sample) to 335.5 eV for the two reduced samples. This value of binding energy (Pd 3d5/2 at 335.5 eV) suggests that the oxidation state of Pd is zero in both reduced catalysts.[5,24]

It is worth noting that our results are very close to those previously obtained in a study on nonsupported Pd_4S nanoparticles where a zero oxidation state for both Pd and S was found by XPS measurements.[15] In this latter work, the possibility of charge transfer from Pd to S in Pd_4S is also discussed based on a marginal shift of the Pd 3d binding energy with respect to that of pure Pd. In our case, the difference between the value of 335.5 eV for the Pd $3d_{5/2}$ in the reduced $PdSO_4$−HHTox and $PdCl_2$−HHT- SO_3H catalysts and those found in the literature[5,24] for Pd zero is of 0.2 eV as maximum, which is within the error of determination. Therefore, the XRD-identified Pd_4S phase may be described as an alloy type compound with structure basically similar to Pd^0 where the S atoms occupy substitutional sites resulting in some distortions. In addition, it has been reported that Pd_4S can intrinsically

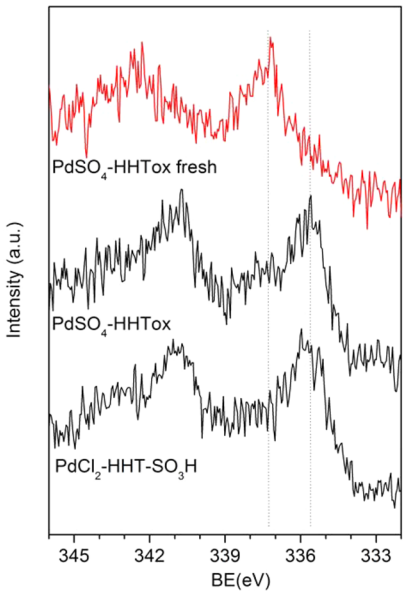

Figure 4. XPS spectra of the Pd 3d core level for the $PdSO_4$−HHTox and $PdCl_2$−HHT- SO_3H catalysts reduced at 250 °C in hydrogen and the fresh $PdSO_4$−HHTox sample.

behave as a metal, especially in relation to conducting electrons.[25] The values of mean particle size estimated using the Scherrer equation for the Pd_4S phase are of 17.4 and 10.8 nm for $PdSO_4$−HHTox and $PdCl_2$−HHT-SO_3H catalysts reduced at 250 °C, respectively.

Figure 5 shows the evolution of Pd phases of reduced catalysts under butadiene hydrogenation reaction atmosphere at different temperatures and during H_2/H_2 + Bd/H_2 alternate exposure. Once the catalysts were treated in hydrogen at 250 °C, the temperature was reduced to the corresponding reaction temperatures, which were selected for each catalyst within the range of activity shown in Table 1.

The structural study of the reference $PdCl_2$−HHTox sample reveals at room temperature no changes in the lattice parameters of the formed β-Pd hydride phase during the H_2/H_2 + Bd/H_2 alternate exposure. The same applies for the Pd phase at 150 °C which remains unchanged under the different atmospheres. MS analysis under H_2 + Bd atmosphere confirms that both phases of palladium (β-Pd hydride and metallic Pd) are active at the corresponding reaction temperatures. In Figure 5, signals labeled m/z = 39, 41, and 43 are plotted. The first one is associated with the reactant, butadiene, whereas the other two correspond to the reaction products butenes and butane, respectively. The nonselective total hydrogenation of butadiene and major production of butane were observed. This $PdCl_2$−HHTox sample does not have preferential growth of particles along a given crystallographic direction and is made of spherical nanoparticles (see HRTEM micrographs at Figure 1 and at Supporting Information, Figure S2); thus, it could be assumed that a major fraction of the most thermodynamically stable (111) surface is exposed. The earliest comparative studies with different nanostructured Pd catalysts established that the (100) facets are more active for the butadiene hydrogenation, but they are also more selective for terminating the reaction at the butenes than the (111) surfaces.[26,27] Similarly, Silvestre et al.[7] also observed that (110) surfaces are particularly selective for the hydrogenation of dienes into alkenes. Moreover, selective partial hydrogenation of dialkenes and alkynes to alkenes on Pd

DOI: 10.1021/acscatal.5b00896
ACS Catal. 2015, 5, 5235−5241

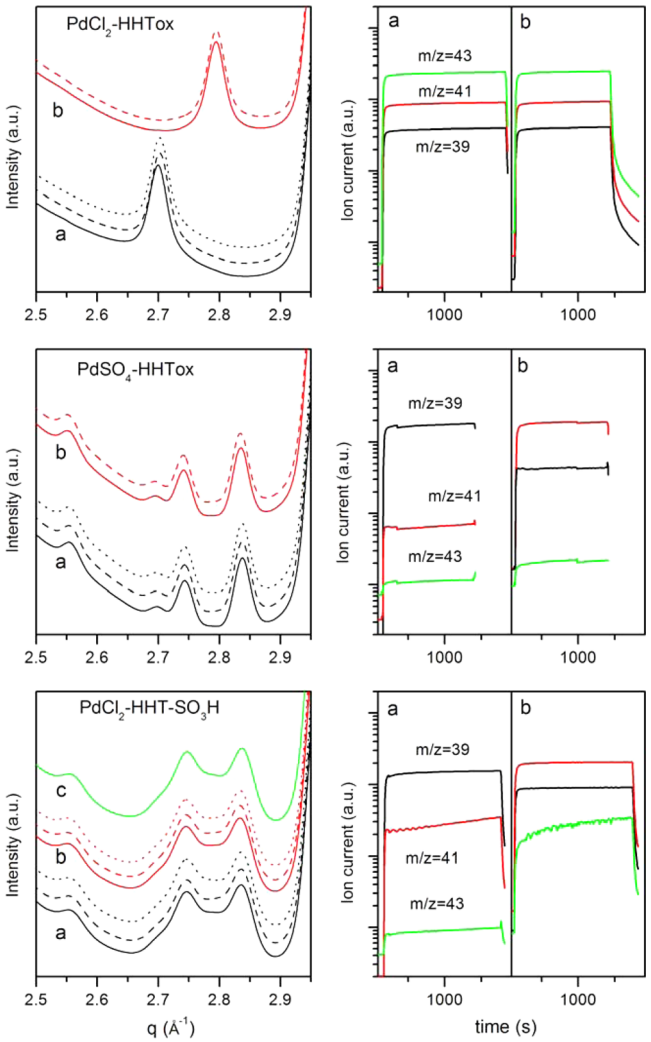

Figure 5. HEXRD patterns obtained under consecutive H_2 (—), H_2+Bd (- - -), H_2 (...) atmospheres at several constant temperatures and MS results for selected m/z values under H_2 + Bd. Upper panels: PdC_{l2}-HHTox; a: RT, b: 150 °C. Middle panels: $PdSO_4$−HHTox; a: 100 °C, b: 160 °C. Lower panels: $PdCl_2$−HHT-SO_3H; a: 100 °C, b: 140 °C, c: RT.

catalysts has been related with the formation of subsurface layers of Pd carbide (PdC_x), which limits the diffusion of hydrogen and its availability for hydrogenation reaction.[2,9] The isotropic palladium nanoparticles and the absence of Pd carbide phase (detectable in our experimental conditions for a chemical composition PdC_x, with x larger than 0.002)[28] in the $PtCl_2$−HHTox sample upon exposition to the reaction atmosphere at both temperatures (RT and 150 °C) likely explain its unselective catalytic behavior in the butadiene hydrogenation.

The same HEXRD study carried out over $PdSO_4$−HHTox sample reveals also no structural changes in the phase formed during reduction in hydrogen at 250 °C (Figure 5). Thus, the lattice parameters of the Pd_4S phase remains constant, with variations far below the estimated error of ±0.004 Å, during the time of exposition to reaction mixture and switching to hydrogen at both 100 and 150 °C temperatures. In addition, the MS analysis shows, in agreement with the previous steady-state catalytic studies (Table 1), the high selectivity of the catalyst for the partial hydrogenation of butadiene (m/z = 39) into butenes (m/z = 41). Theoretical investigations of H_2 dissociation on the faces of Pd_4S indicate that dissociation barriers are higher than on Pd (111) face, although low enough to allow the partial hydrogenation of dialkenes and alkynes.[29] Therefore, the Pd_4S phase constitutes an active and selective catalytic phase for partial hydrogenation of polyunsaturated hydrocarbons. Interestingly, the palladium sulfide phase is stable during the H_2/H_2 + Bd/H_2 alternate exposures, whereby regeneration of the catalyst with further feeding a sulfur compound, common practice in hydrorefining plants,[1,3] is likely unneeded. The stability of the Pd_4S phase in the $PdSO_4$−HHTox catalyst under reaction conditions is also proved by a long-term catalytic run performed in fixed bed reactor at 100 °C, with 60 mL of the reaction mixture of H_2:Bd:N_2 (10:2:88) and 30 mg of catalyst (Figure 6). It can be seen that activity and selectivity were maintained during the run.

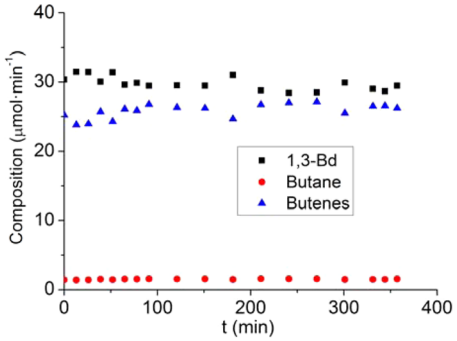

Figure 6. Stability test carried out at 100 °C on the $PdSO_4$−HHTox catalyst.

Similarly, in the case of the $PdCl_2$−HHT-SO_3H sample (Figure 5 lower panels), the two phases (79% Pd_4S and 21% Pd) formed after reduction treatment remain unchanged upon H_2/H_2 + Bd/H_2 alternate exposures at 100 and 140 °C. Strikingly, when the temperature is cooled to room temperature in hydrogen atmosphere the foreseeable change in the Pd metal d spacing due to the β-Pd hydride phase formation does not occur. Likely, we have nanoparticles with a Pd@Pd_4S core−shell nanostructure where the Pd_4S shell hinders the diffusion of hydrogen to the Pd core. It is known that the H_2 permeability of Pd_4S is more than 1 order of magnitude lower than that of metallic Pd.[30]

Considering the results of our temperature-programmed reduction in hydrogen experiments where we used HEXRD coupled with MS experiments (Figure 2) and in agreement with the literature,[31] we believe that the sulfidation process is a stepwise process which comprises (1) decomposition of H_2S and SO_2 precursors (sulfate anions and sulfonic groups for $PdSO_4$−HHTox and $PdCl_2$−HHT-SO_3H, respectively), (2) adsorption of these gaseous molecules on the surface of the metallic Pd nanoparticles initiating the sulfidation at the surface at around 150 °C, and lastly, (3) progressing of sulfur into the bulk of Pd particles. Hence, the formation of bulk Pd_4S nanoparticles in the reduced $PdCl_2$−HHT-SO_3H catalyst is likely precluded for the limited decomposition, at temperatures below 250 °C, of the sulfonic groups covalently anchored to the surface of the support (see Supporting Information, Figure S1).

The MS analysis under reaction (Figure 5 lower panels) shows a high selectivity to partial hydrogenation at 100 °C, whereas at 140 °C, some proportion of butane is produced. Moreover, this $PdCl_2$−HHT-SO_3H sample, in agreement with

DOI: 10.1021/acscatal.5b00896
ACS Catal. 2015, 5, 5235−5241

catalytic studies (Table 1), is somewhat more active than the $PdSO_4$−HHTox. The higher catalytic activity of the former can be clearly attributed to the larger dispersion of the active Pd_4S phase. Moreover, the smaller particle size in this sample turns into a higher proportion of unsaturated sites at edges and corners on where the H_2 dissociation barrier becomes likely reduced and therefore the partial hydrogenation of dialkenes deprived at higher reaction temperatures.[2,29]

In summary, we have developed a simple and green method to produce an active, very stable, and highly selective catalyst for the butadiene hydrogenation (here named $PdSO_4$−HHTox) based on the pure Pd_4S phase supported on carbon nanofibers. The palladium sulfide precursor is a common palladium sulfate salt impregnated on the carbon support. The catalyst is produced in a single step via reduction process in hydrogen atmosphere without further sulfidation.

4. CONCLUSIONS

On the basis of our observations, by combining HEXRD and MS measurements, we propose that the reduction under hydrogen of the carbon supported palladium sulfate precursor, $PdSO_4$−HHTox sample, provides the Pd_4S-based catalyst with superior selectivity to partial hydrogenation of dialkenes. This approach supposes an easy and confident method to synthesize a well-defined single palladium sulfide structure. Contrarily to Pd metal, where thermodynamically nonstable surfaces and morphologies are required to obtain the desired selectivity, here we present a Pd_4S phase with significant activity, appropriate selectivity, and high stability under reaction conditions. Moreover, an effect of particle size of the Pd_4S phase on the selectivity to partial hydrogenation has been also observed; that is, crystallites above 11 nm are likely needed for a full selectivity to partial hydrogenation of butadiene. Lastly, we note that the experimental procedure to obtain the sulfide phase is rather simple and does not require in situ sulfidation steps.

■ ASSOCIATED CONTENT

Supporting Information

The Supporting Information is available free of charge on the ACS Publications website at DOI: 10.1021/acscatal.5b00896.

TPD−MS profiles of the HHTox and HHT-SO_3H supports; TEM micrographs of the different catalysts; additional HEXRD patterns for the catalysts and pure species; XPS spectra of the S 2p region for the fresh PdSO4-HHTox sample; data derived from application of Rietveld method to HEXRD patterns. (PDF)

■ AUTHOR INFORMATION

Corresponding Authors

*E-mail: aguerrero@ccia.uned.es (A.G.-R.).
*E-mail: irodriguez@icp.csic.es (I.R.-R.).

Notes

The authors declare no competing financial interest.

■ ACKNOWLEDGMENTS

We acknowledge financial support from the Spanish Ministerio de Economía y Competitividad (projects CTQ2011-29272-C04-01 and −03). The ESRF is thanked for granting beamtime at ID15.

■ REFERENCES

(1) Bond, G. C. In *Metal-Catalysed Reactions of Hydrocarbons*; Springer: NewYork, 2005.
(2) Bridier, B.; Karhánek, D.; Pérez-Ramírez, J.; López, N. *Chem. Catal. Chem.* **2012**, *4*, 1420−1427.
(3) McCue, A. J.; Anderson, J. A. *Catal. Sci. Technol.* **2014**, *4*, 272−294.
(4) McKenna, F. M.; Anderson, J. A. *J. Catal.* **2011**, *281*, 231−240.
(5) Cooper, A.; Bachiller-Baeza, B.; Anderson, J. A.; Rodríguez-Ramos, I.; Guerrero-Ruiz, A. *Catal. Sci. Technol.* **2014**, *4*, 1446−1455.
(6) Shao, L.; Zhang, W.; Armbrüster, M.; Teschner, D.; Girgsdies, F.; Zhang, B.; Timpe, O.; Friedrich, M.; Schlögl, R.; Su, D. S. *Angew. Chem., Int. Ed.* **2011**, *50*, 10231−10235.
(7) Silvestre-Albero, J.; Rupprechter, G.; Freund, H. J. *Chem. Commun.* **2006**, 80−82.
(8) Zaera, F. *ChemSusChem* **2013**, *6*, 1797−1820.
(9) Teschner, D.; Borsodi, J.; Wootsch, A.; Révay, Zs.; Havecker, M.; Knop-Gericke, A.; Jackson, S. D.; Schlögl, R. *Science* **2008**, *320*, 86−89.
(10) Xu, W.; Ni, J.; Zhang, Q.; Feng, F.; Xiang, Y.; Li, X. *J. Mater. Chem. A* **2013**, *1*, 12811−12817.
(11) Su, D. S.; Perathoner, S.; Centi, G. *Chem. Rev.* **2013**, *113*, 5782−5816.
(12) Serp, P.; Figueiredo, J. L. In *Carbon Materials for Catalysis*; John Wiley & Sons, Inc.: Hoboken, NJ, 2009.
(13) Zhang, Q.; Xu, W.; Li, X.; Jiang, D.; Xiang, Y.; Wang, J.; Cen, J.; Romano, S.; Ni, J. *Appl. Catal., A* **2015**, *497*, 17−21.
(14) Pang, S. H.; Schoenbaum, C. A.; Schwartz, D. K.; Medlin, J. W. *ACS Catal.* **2014**, *4*, 3123−3131.
(15) Singh, V. V.; Kumar, U.; Tripathi, S. N.; Singh, A. K. *Dalton Trans.* **2014**, *43*, 12555−12563.
(16) Ferri, D.; Newton, M. A.; Di Michiel, M.; Chiarello, G. L.; Yoon, S.; Lu, Y.; Andrieux, J. *Angew. Chem., Int. Ed.* **2014**, *53*, 8890−8894.
(17) Serp, P.; Corrias, M.; Kalck, P. *Appl. Catal., A* **2003**, *253*, 337−358.
(18) Cuervo, M. R.; Asedegbega-Nieto, E.; Díaz, E.; Vega, A.; Ordóñez, S.; Castillejos-López, E.; Rodríguez-Ramos, I. *J. Chromatogr. A* **2008**, *1188*, 264−273.
(19) Almohalla, M.; Morales, M. V.; Asedegbega-Nieto, E.; Maroto-Valiente, A.; Bachiller-Baeza, B.; Rodríguez-Ramos, I.; Guerrero-Ruiz, A. *Open Catal. J.* **2014**, *7*, 1−7.
(20) Bachiller-Baeza, B.; Peña-Bahamonde, J.; Castillejos-Lopez, E.; Guerrero-Ruiz, A.; Rodríguez-Ramos, I. *Catal. Today* **2015**, *249*, 63−71.
(21) Zlotea, C.; Cuevas, F.; Paul-Boncour, V.; Leroy, E.; Dibandjo, P.; Gadiou, R.; Vix-Guterl, C.; Latroche, M. *J. Am. Chem. Soc.* **2010**, *132*, 7720−7729.
(22) JCPDS card no. 73-1387.
(23) Hensen, E. J. M.; Brans, H. J. A.; Lardinois, G. M. H. J.; de Beer, V. H. J.; van Veen, J. A. R.; van Santen, R. *J. Catal.* **2000**, *192*, 98−107.
(24) Brun, M.; Berthet, A.; Bertolini, J. C. *J. Electron Spectrosc. Relat. Phenom.* **1999**, *104*, 55−60.
(25) Radha, B.; Kulkarni, G. U. *Adv. Funct. Mater.* **2010**, *20*, 879−884.
(26) Berhault, G.; Bisson, L.; Thomazeau, C.; Verdon, C.; Uzio, D. *Appl. Catal., A* **2007**, *327*, 32−43.
(27) Piccolo, L.; Valcarcel, A.; Bausach, M.; Thomazeau, C.; Uzio, D.; Berhault, G. *Phys. Chem. Chem. Phys.* **2008**, *10*, 5504−5506.
(28) Newton, M. A.; Di Michiel, M.; Kubacka, A.; Fernandez-Garcia, M. *J. Am. Chem. Soc.* **2010**, *132*, 4540−4541.
(29) Miller, J. B.; Alfonso, D. R.; Howard, B. H.; O'Brien, C. P.; Morreale, B. D. *J. Phys. Chem. C* **2009**, *113*, 18800−18806.
(30) O'Brien, C. P.; Gellman, A. J.; Morreale, B. D.; Miller, J. B. *J. Membr. Sci.* **2011**, *371*, 263−267.
(31) Diaz-Chao, P.; Ferrer, I. J.; Ares, J. R.; Sanchez, C. *J. Phys. Chem. C* **2009**, *113*, 5329−5335.

DOI: 10.1021/acscatal.5b00896
ACS Catal. 2015, 5, 5235−5241